

Permeation of Low-Z Atoms through Carbon Sheets: Density Functional Theory Study on Energy Barriers and Deformation Effects

Stefan E. Huber*, Andreas Mauracher and Michael Probst*

Institute of Ion Physics and Applied Physics, University of Innsbruck, Technikerstraße 25, 6020 Innsbruck, Austria

* Corresponding authors. Stefan E. Huber: E-mail: s.huber@uibk.ac.at, phone: +43 512 507 6247, Fax: +43 512 507 2922. Michael Probst: E-mail: Michael.probst@uibk.ac.at, phone: +43 512 507 6260, Fax: +43 512 507 2922.

Abstract

Energetic and geometric aspects of the permeation of low-Z atoms through graphene sheets are investigated. Energy barriers and deformations are calculated via density functional theory for the permeation of H, He, Li and Be atoms at several surface sites and at a hollow site for atoms B, C, N, O, F, and Ne atoms. Graphene is modeled by large planar polycyclic aromatic hydrocarbons and the convergence of both energy barriers and deformation curves with increasing size of these hydrocarbons is investigated. Effective energy curves are summarized for the atoms under consideration in three different interaction regimes realized different geometrical constraints. In addition to the bare graphene model, the interaction between low-Z atoms and 100% hydrogenated coronene as a model for graphane is also investigated. The barriers range from 5 eV ($1 \text{ eV} = 1.602 \times 10^{-19} \text{ J}$) for H to 20 eV for Ne. Facilitation of the permeation by temporary chemical bonding is observed for O and C and for B and Be when interacting with hydrogenated coronene.

1. Introduction

Many critical issues in present thermo-nuclear fusion research are closely related to the topic of plasma wall interaction [1]. For example, in order to predict if the constraints on tritium retention are within the limits, the interaction details of hydrogen (and D and T) atoms and their ions with the wall materials should be known. These issues are even more complicated in ITER (International Thermonuclear Experimental Reactor) where several materials are planned to be used, in one scenario graphite for the divertor plates, tungsten in the upper divertor and dome and beryllium in the main wall.

In such a tokamak the so-called scrape-off layer (SOL) plasma interacts with the plasma facing components (PFCs). The electronic temperature of the SOL located outside the last closed flux surface is much lower than that of the core plasma where the fusion process should be maintained. The bombardment of the walls by hydrogen atoms and/or ions gives rise to the pollution of the plasma by impurities expelled from the PFCs that can go far into the plasma through the surfaces of the magnetic field. The divertor region acts as power and particle exhaust in order to maintain a pure core plasma [2]. For this region in ITER, carbon fiber composite is envisaged, amongst other choices. In addition to ubiquitous plasma species as H (or D and T) and the fusion product He, PWI gives rise to impurities of C, Be and W [2-5]. Furthermore, techniques like wall conditioning [6-12] and impurity seeding [13-17] generate an even greater variety of plasma impurities consisting of, e.g. Li, B, N, O, Si, Ne, Ar, Xe. Understanding the interaction of these impurities with graphite surfaces is therefore important if one wants to control the PWI processes in a mixed-material fusion device such as ITER.

Because of the abundance of H, D and T, mainly the interaction of these particles with carbon-based materials has been studied extensively by computational techniques like molecular dynamics (MD) simulations [18-23]

and quantum-chemical methods [24-26]. Besides that, there exist various studies of other atom/molecule/ion-surface interactions possibly relevant for magnetic fusion [27-31].

Our work is of the second type. We performed quantum mechanical DFT calculations of energy profiles and geometric features of atom/graphene systems. Such profiles explain certain characteristics of the systems, especially the different behavior depending on size and electronic structure of the particles. To our knowledge, there has never been an overall atomistic investigation of the interaction and transmission of atoms with and through graphene sheets.

Energy profiles can also be used as effective energy functions that are needed in classical MD simulations to describe the interactions between particles. These potentials are typically derived from equilibrium situations [32], but are often of poor accuracy when applied to non-equilibrium processes and, especially, systems under extreme conditions [28]. There is much need for robust reactive analytical potentials of any level of sophistication.

Graphite is a multilayer consisting of two-dimensional graphene sheets. Thus, the interaction of atoms and/or molecules with graphitic surfaces can to some extent be modeled by their interaction with graphene. Physisorption and chemisorption of hydrogen and of a variety of other atoms on graphite surfaces or on graphene has already been studied extensively by DFT methods [33-37]. In this work, we do not focus on these processes but on the permeation of various fusion-relevant atoms through graphene. We investigate the energy barriers arising from the repulsive forces between valence electrons as well as the deformation of the graphitic surface in the vicinity of the permeation site. For the light atoms H, He, Li, and Be we investigate permeation at three surface sites: The 'hollow site' in the center of one aromatic ring; the 'bridge site', above the midpoint of a carbon-carbon bond; and the 'top site' on top of one carbon atom. For the higher-Z atoms B to Ne, we only investigate permeation at the hollow site.

In tokamaks, interaction of high-energy ions with carbon-based PFCs is at the origin of physical sputtering whereas low energy (hydrogen) atoms are responsible for the chemical erosion of carbon surfaces. The present work deals only with neutral atomic species. Furthermore the energy surfaces are by definition time-independent although they drive the dynamics, and therefore they are identical for all isotopes of one element.

After briefly summarizing the numerical methods in section II, we discuss our results on the adiabatic permeation of low-Z atoms H to Ne through graphene models at the hollow site in section III A. This is followed by analogous analyses of bridge and top sites in sections III B and III C for the atoms H to Be. In sections III D and III E we discuss the different interaction regimes and the interaction of atoms with hydrogenated hydrocarbons as models for graphane [38]. Finally, in section IV, a summary is given.

2. Method

2.1 Cluster Model

We use a cluster approach where graphite is modeled by polycyclic aromatic hydrocarbons (PAHs). This avoids some problems associated with periodic calculations but it requires that the cluster model has the same or similar properties as the extended system. We discuss this issue in section III B. The PAHs can be thought as small pieces of graphene sheets with the free valences of the dangling bonds saturated by hydrogen. Vice versa, a graphene sheet can be interpreted as an infinite PAH molecule. Successful utilization of PAH molecules in modeling graphitic surfaces has been reported earlier [39]. The PAHs used in our work are (i) benzene with six carbon atoms, (ii) anthracene with 14 carbon atoms, (iii) pyrene with 16 carbon atoms, (iv) triphenyl with 18 carbon atoms, (v) coronene with 24 carbon atoms, (vi) circumpyrene with 42 carbon atoms and (vii) circumcoronene with 54 carbon atoms (Fig. 1).

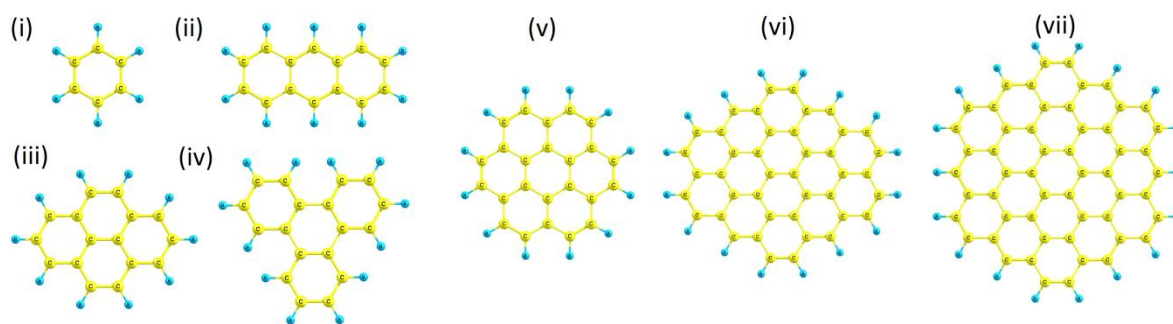


Figure 1: PAH molecules used as graphene models.

The interaction energy between these PAH molecules and the low-Z atoms is calculated by the density functional methods described in the next paragraph as a function of the distance z between the atom and the undisturbed PAH plane ($z=0$). This is done numerically by varying z in steps of 0.2 \AA , where $1 \text{ \AA} = 10^{-10} \text{ m}$.

We considered three limiting cases: (a) the ‘adiabatic’ situation where at each distance of the approaching atom from the surface the system geometry, except this distance, is fully relaxed. The hydrogen atoms at the PAH border remain in the original plane and define the value of z . This results in a bending of the cluster surface and a stretching or shortening of individual C-C bonds. As a measure of the amount of deformation we took the displacement of carbon atoms from the original PAH plane and the change of the C-C bond length in the vicinity of the permeation site. (b) differs from the ‘adiabatic’ situation in that the carbon atoms remain restricted in their original plane but can move in the two other dimensions. Finally, in (c) the PAH molecule remains rigid in its equilibrium geometry.

Energies and geometries were obtained from DFT calculations with the B3LYP [40] and PBE0 [41] functionals. Both are hybrid functionals and include a mixture of Hartree-Fock exchange and DFT exchange-correlation. The widely used B3LYP functional has been constructed semi-empirically by fitting its three parameters to experimental data. The parameter-free PBE0 functional is based on the fulfillment of a number of physical constraints. The independent and complimentary foundation makes it interesting to use both functionals and to compare their results. A well-known deficiency of such density functionals is their inability to describe dispersion interactions. This would become important when one is, for example, interested in the shallow van-der-Waals attraction between surfaces and weakly interacting atomic species such as He and Ne. Even if the neglect of dispersion is not expected to be an issue for the energy barriers we are mostly interested in, we have recalculated 10 potential energy curves with the wB97XD functional which can account for dispersion interactions [42]. For simplicity, we do not include this in the following discussion but just mention that, comparing with the B3LYP and PBE0 results, we found similar shapes of the energy profiles and similar values for their energy maxima for all three. The deviations between the two types of functionals were below 10%. The wB97XD interaction energies are slightly larger than the ones from B3LYP and PBE0. In the DFT calculations the electron densities are expanded in basis sets. Test calculations with large and small basis sets show that the split-valence basis sets 3-21G [43] and 6-31G [44] we used here overestimate the barrier maxima by up to 10% with respect to larger basis sets. Taking into account the underestimation of the maxima due to the functionals discussed above and other approximations, for example the finite step size, we estimate the total accuracy of our method to be about 10-15%. All calculations have been performed with the Gaussian 09 software [45].

3. Results

3.1 Energy decomposition

The planar hydrocarbon molecule becomes distorted when the impinging atom approaches. In most cases, it bends away from the atom, outwards of the original plane in order to reduce the repulsion between the electrons. The atom-PAH interaction energy ΔE is then

$$\Delta E = E_{\text{tot}}(\text{A-PAH}) - E_{\text{tot}}(\text{PAH}) - E_{\text{tot}}(\text{A})$$

where E_{tot} is the total energy of the relaxed system. ΔE can be divided into the interaction energy between the fragments at their positions and geometries and the energy required for the deformation of the PAH molecule due to this interaction. For small distances between the contaminant atom and the hydrocarbon molecule the interaction energy is positive, giving rise to an energy barrier with a certain shape characteristic for the model.

3.2 Convergence of energy and deformation with increasing model size

In order of the cluster calculations to be used to model the interactions between atoms and extended graphene, the energy profiles and especially their maxima must converge for increasing size of the PAH molecule towards graphene as an infinitely sized PAH molecule. In the following we present simple considerations and tests that give rise to the assumption that this is indeed the case.

- For larger distances the contaminant atom and the PAH weakly attract each other by dispersion-like interactions that typically scale as or similar to $1/r^6$. For small distances the interaction will be strongly repulsive e.g. as the $1/r^{12}$ in a Lennard-Jones model. In between chemical bonding can occur which is also short-range and directional. All these interactions are short-ranged.
- Thus, the interaction energy is mainly given by the nearest carbon atoms, i.e. the atoms of the carbon ring in case of permeation at the hollow site at its middle. Since on the other hand the number of carbon atoms increases with the square of the distance from these carbon atoms, the interaction energy will approach some constant value if the PAH gets larger. The underlying condition is that the PAH properties relevant for the interaction with incoming particles itself do not change as a property of their size. In case of PAHs this is valid to a good degree, in contrast, for example, to metal nanoparticles where surface bonding interactions are strongly related to their size.
- The deformation energy should in principle approach a constant value for infinite sized PAH molecules (graphene). Each carbon atom has 1.5 bonds to neighboring carbons – three bonds shared between two atoms each. If we employ a simple model where each C-C bond is a harmonic spring with spring constant k , the displacement of one carbon atom creates a counteracting force proportional to an overall spring constant

$$K = k \left(\frac{1}{n} + \frac{1}{n^2} + \dots + \frac{1}{n^N} \right)^{-1}$$

where n is the number of bonds to neighboring carbons and N is the total number of carbons constituting the PAH molecule. Since K converges to $k \times (n-1)$ for $N \rightarrow \infty$ and $n > 1$, the total displacement of a carbon atom on which a force from an approaching particle is exerted remains finite. Therefore, the energy barrier between atom and PAH will converge to the atom/graphene barrier with increasing PAH size. This can be rationalized by considering that in a small PAH with fixed border atoms larger changes of curvature and bond structure will be induced than in a large one but that this is just compensated by a larger area and number of bonds affected in the large PAH.

In Fig. 2a the maximum displacement from the original molecular plane is plotted against the number of carbon atoms of the PAH molecule. The circles give the results for H to Be permeating PAH molecules at the hollow site. The solid lines are functions of the form $f(x) = a(1 - e^{-bx}) + c$, fitted to the density functional data. x denotes the number of carbon atoms and a - c are fitting parameters. One sees a slow convergence of the bending parameter. This is due to the fact that the boundary region has a large influence in case of small PAH molecules. If instead the bending parameter is plotted as a function of the number of atoms not connected to the boundary (Fig. 2b), the convergence is faster and the fit functions are better approximations to the data points. However, it turns out the energy barrier heights as well as the maxima in the curves describing the change in C-C bond length convergence much faster as can be seen from the results discussed in the following.

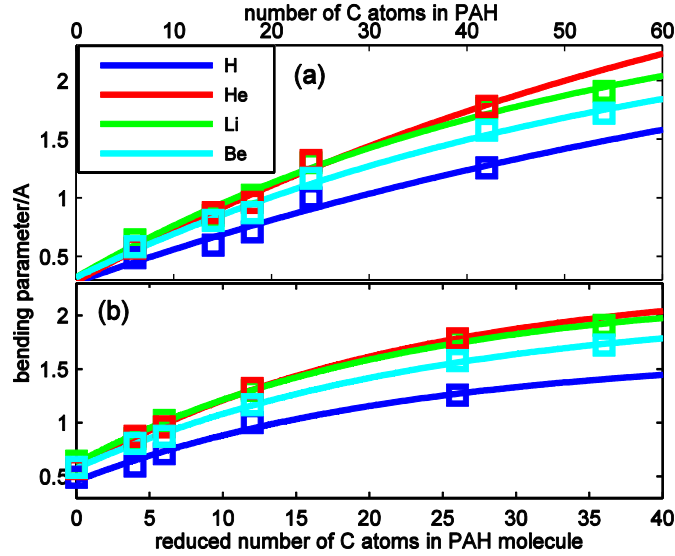


Figure 2: Bending parameter for different atom-molecule interactions plotted versus the number of carbon atoms in the PAH molecule in (a) and versus a reduced number of carbon atoms in (b). The better fit in (b) is explained in the text.

3.2 Adiabatic permeation at hollow site

Our calculations correspond to the physical situation in which the surface structure relaxes much faster than contaminant atom approaches it. One can call this the adiabatic interaction regime. Two other extreme cases, the in-plane regime as well as the ultra-fast regime, are also considered and will be discussed in detail in Sec. III. E. In the following we discuss the energy barriers and deformation effects for adiabatic permeation of the atoms H up to Ne through different PAH molecules as models for graphene at hollow site. The energy barriers can roughly be divided according to their shape into ‘regular’ ones and more complex (or ‘irregular’) ones. The regular energy barriers are characterized by a steep increase of the energy at about 2 Å distance between the contaminant atom and the PAH molecule under consideration up to a maximum in energy and a steep decrease (jump) afterwards back to about zero energy. H, He, Li (concerning the results obtained with B3LYP), Be, F and Ne were interacting with the PAH in this ‘regular’ way. The ‘irregular’ energy barriers are discussed individually for the various types of contaminant atoms. The energy barriers for adiabatic permeation through the three largest PAH molecules (coronene, circumpyrene and circumcoronene) at a hollow site are shown in Fig. 3. The characteristic energy maxima for permeation through coronene (if available) are summarized in Table 1. The maxima, i.e. the heights of the energy barriers, approximately follow the order of the atoms in the periodic table. Exceptions are helium with a maximum of about 12 eV, where $1 \text{ eV} = 1.602 \times 10^{-19} \text{ J}$, which is due to its closed shell configuration, and carbon and oxygen. Their ability to form chemical bonds with the surface lowers the barrier height for most distances, compared to inert atoms of similar van-der-Waals radii. Except for these atoms, the energy maxima range from about 5 eV in case of hydrogen up to about 20 eV for neon. The energy barrier for hydrogen is in reasonable agreement with earlier DFT studies [25] but to the best of our knowledge, information for the other elements has been lacking.

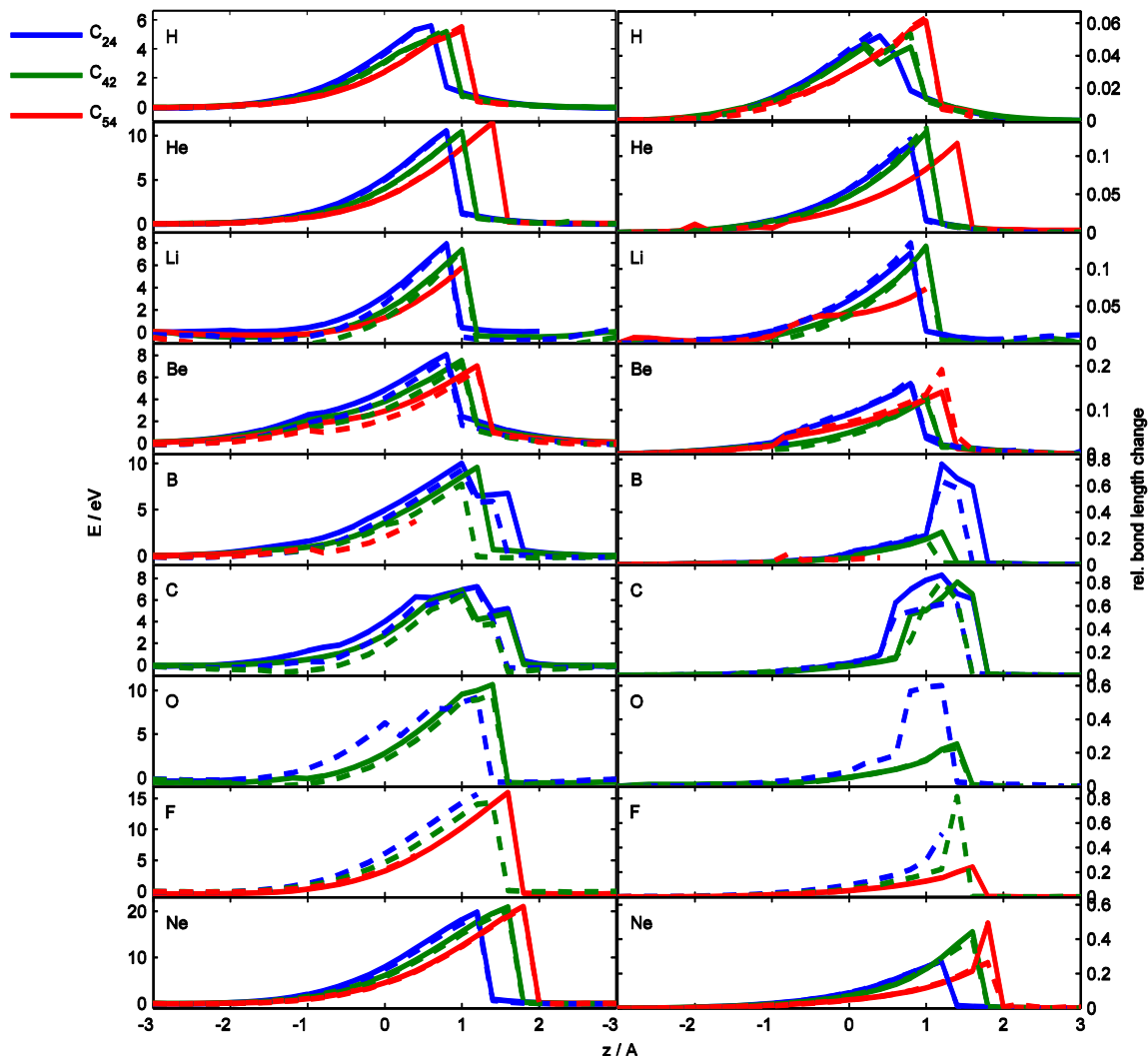


Figure 3: Energy barriers (left) and relative change in C-C bond length in the vicinity of the permeation site (right) for the permeation of H to Ne through coronene (blue), circumpyrene (green) and circumcoronene (red). Results are shown for the B3LYP (solid lines) and PBE0 (dashed lines) density functionals.

In addition to the energetics we also tried to quantify the deformation of the PAH molecule. As a simple measure, the relative change in the C-C bond length in the vicinity of the permeation site is calculated as a function of the z-coordinate of the contaminant atom (Fig. 3.). The ‘irregularities’ in the energy barriers are mostly reflected in the deformation curves. Values for the maxima are summarized in Table 1. Also the maximal deformation follows approximately the order of the atoms in the periodic table (except for carbon and oxygen, see the discussion below). The values range from small changes of 5-6% for hydrogen up to about 30% in case of neon and even up to 80-90% in some cases that are discussed below.

Table 1: Energy maxima, E_{max} , and maxima of the relative change of the C-C bond length, D_{max} , for the permeation of H to Ne through coronene. Results for N are missing due to convergence problems. The values correspond to the two functionals B3LYP/PBE0.

Atom	H	He	Li	Be	B	C	O	F	Ne
$E_{\text{max}}/[\text{eV}]$	5.7/-	10.6/10.4	7.9/7.8	8.1/7.6	10/9.3	7.2/6.9	-/9.2	16 ^b /14.3 ^c	19.9/19
$D_{\text{max}}/[\%]$	5.2/-	11.5/12.2	12.1/13.5	16/16.8	75 ^a /64 ^a	86/60	-/60	24 ^b /82 ^c	27/27

^a large values due to asymmetric deformation; characteristic values for symmetric deformations are about 20%

^b values obtained from permeation through circumcoronene

^c values obtained from permeation through circumpyrene

It turns out that the results for both the energies and the deformations converge fast with increasing size of the PAH molecules. Whereas there can be larger differences in the two curves for the small molecules as benzene, anthracene or triphenyl, they are very similar for coronene, circumpyrene and circumcoronene, at least for the maxima. It should also be kept in mind that due to the methods and basis sets used and due to the finite step size in the energy scan, the accuracy of the method is not better than 10-15%, as outlined in Sec. II. Encouragingly, the B3LYP and PBE0 functionals give mostly that are well inside this accuracy interval the maxima of the energy and deformation curves. In a few cases, however, they behave differently in regions far from the maximum.

For lithium, PBE0 predicts strong adsorption of Li at the hollow site of the graphene model with deep minima before and after the maximum. Since B3LYP gives only shallow minima in these regions, a more quantitative assessment of adsorption energies would require higher-level calculations. Since we are focusing on the process of permeation, we did not pursue this.

In case of boron the results from the two functionals differ most, about 20% at the energy maxima. The curve for circumcoronene is missing due to convergence problems which are more common for higher-Z contaminant atoms and especially when open-shell configurations are present. A pronounced maximum in the deformation curve for permeation through coronene can be seen which stems from an asymmetry in the way this PAH is deformed, see Fig. 4. This asymmetry is also responsible for the unusual ‘buckle’ in the respective energy curve (Fig. 3).

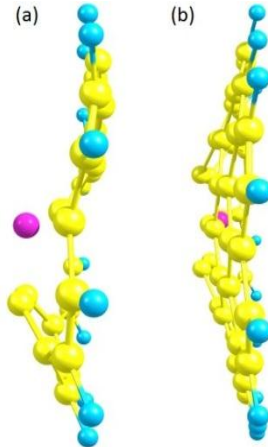


Figure 4: Difference between permeation of B (violet sphere) through (a) coronene and (b) circumpyrene. The asymmetrical deformation caused by bond formation can be seen in (a).

For carbon and oxygen, larger deviations between the two methods are observed. This is not surprising since both energy and deformation curves reveal relative kinks, buckles and additional minima occurring in front of the steep increase to the energy maximum. This is a consequence of the reactivity of these elements with the carbon atoms and show the formation and breaking of chemical bonds. It can be analyzed by decomposing the total energy barrier into the energy that is stored in the deformation of the PAH molecule and the remaining interaction energy, which can be done by calculating the energies of the deformed PAH molecules alone at each scan step. We carried out this decomposition for coronene (Fig. 5). One sees that the systems that give rise to ‘irregular’ curves are those which are attractive at some distances. This happens in the B-, C-, and O-PAH

systems. For all the other systems under consideration (except for Li-PAH / PBE0 results as discussed above) the interaction energy contribution is always positive.

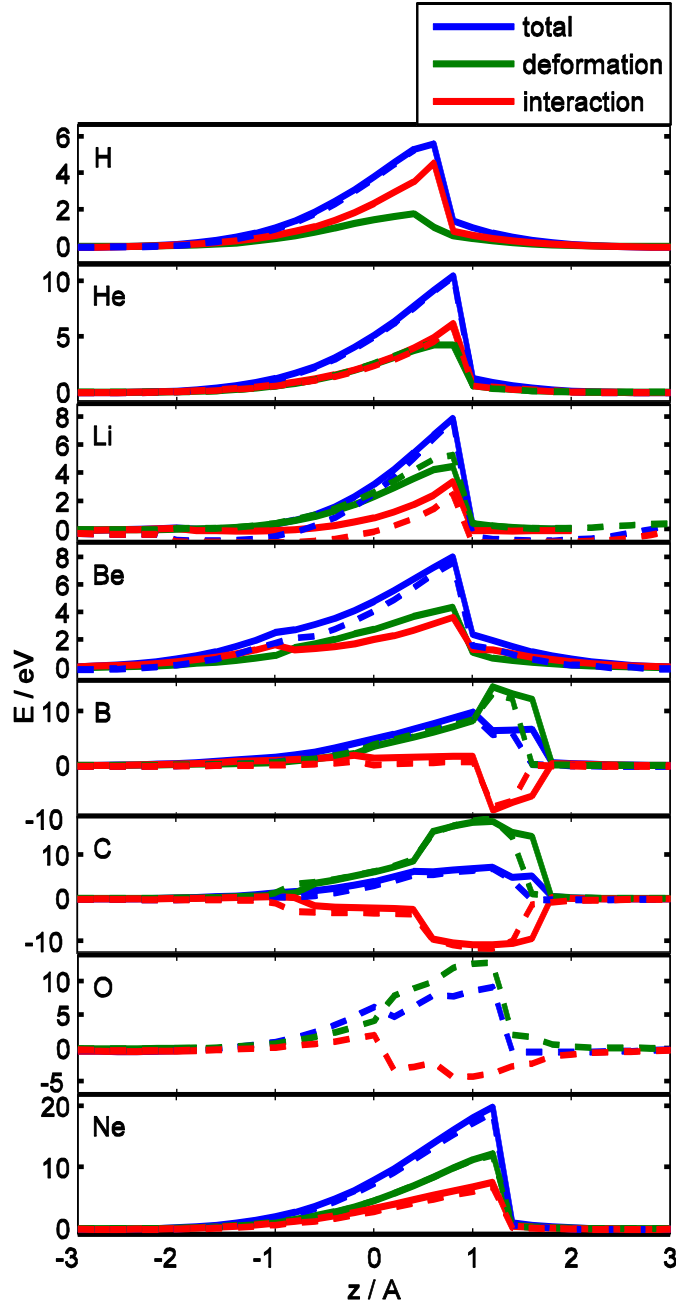


Figure 5: Decomposition of total energy barrier (blue) into 'pure' interaction energy (red) and deformation energy (green) for the atoms H-C, O and Ne permeating coronene. Results are shown for B3LYP (solid lines) and PBE0 (dashed lines).

Due to convergence problems the data obtained from the DFT calculations for nitrogen is not included in Fig. 5. For nitrogen in the two other interaction regimes, see Sec. III. E.

3.3 Adiabatic permeation at a bridge site

For H, He, Li and Be the interaction at bridge and top sites has also been investigated. The total energy barriers and relative changes in C-C bond length in the vicinity of the permeation site are quite similar to the ones discussed above. The differences that arise from the higher energy requirement to break a C-C bond compared to the one to enlarge a hexagonal opening are discussed here.

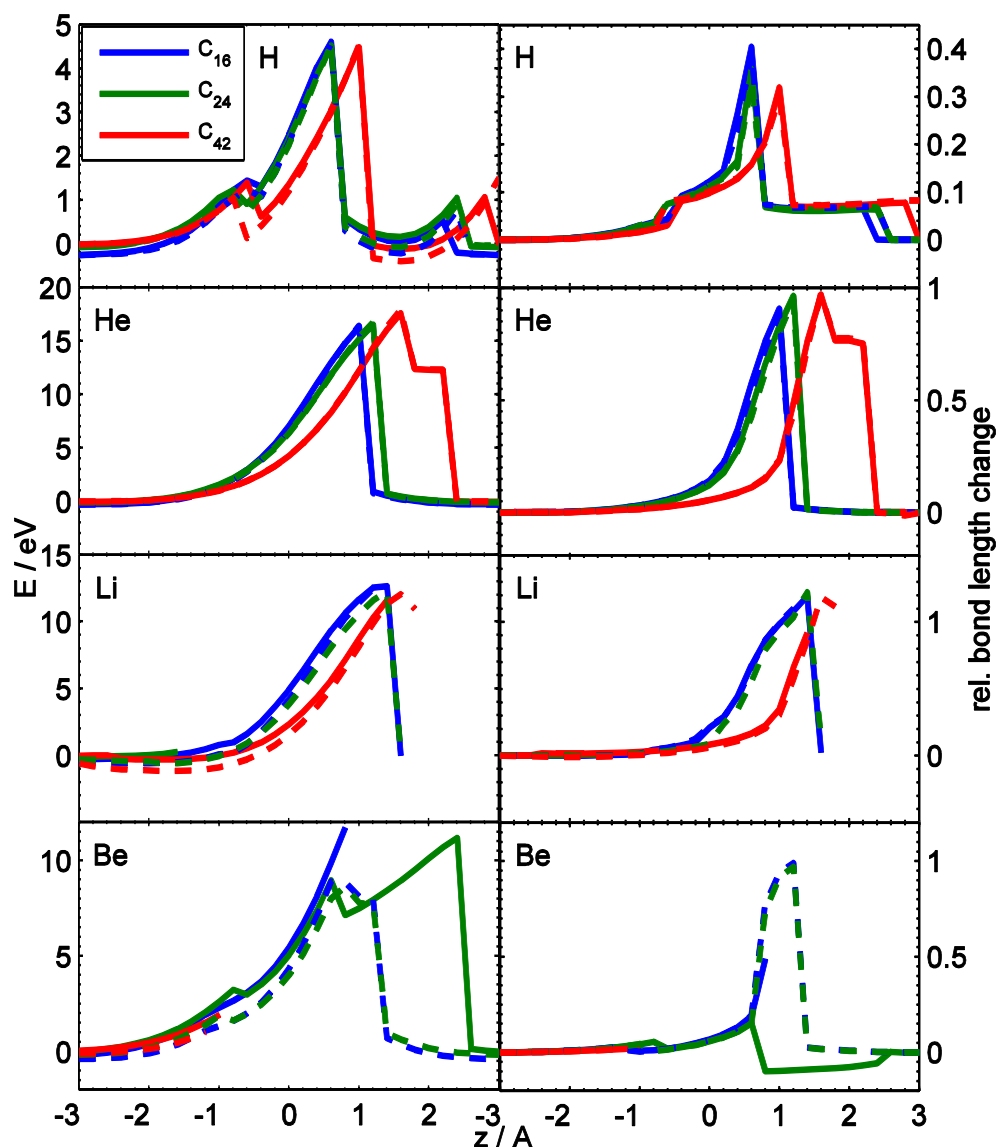


Figure 6: Energy barriers and relative change in C-C bond length in the vicinity of the permeation site for adiabatic permeation through anthracene (blue), coronene (green) and circumpyrene (red) at a bridge site for H, He, Li and Be. Results are shown for B3LYP (solid lines) and PBE0 (dashed lines).

In Fig. 6 the results of the calculations for H and the three PAH molecules are given. As in case of the hollow site, B3LYP and PBE0 yield similar results. The important difference, however, are the two additional maxima in both curves. The closer approach of H to the C-C carbon atoms causes a tetrahedral arrangement when H approaches to about 1 Å (Fig. 7). The same happens when H leaves at the other side of the PAH where the tetrahedral configuration is maintained until $z=2.2-2.8$ Å, leading to the energy maximum in that region. Simultaneously with the C-H bond formation the C-C bond is weakened and the C-C distance becomes much larger. The energy maximum is almost equal for all three kinds of PAHs. The heights of these maxima (about 4.5

eV) are smaller than the corresponding maxima for the hollow site case (about 5.7 eV). One sees that the penetration of H through the PAH is mediated by C-H bond formation. This is only the case for hydrogen.

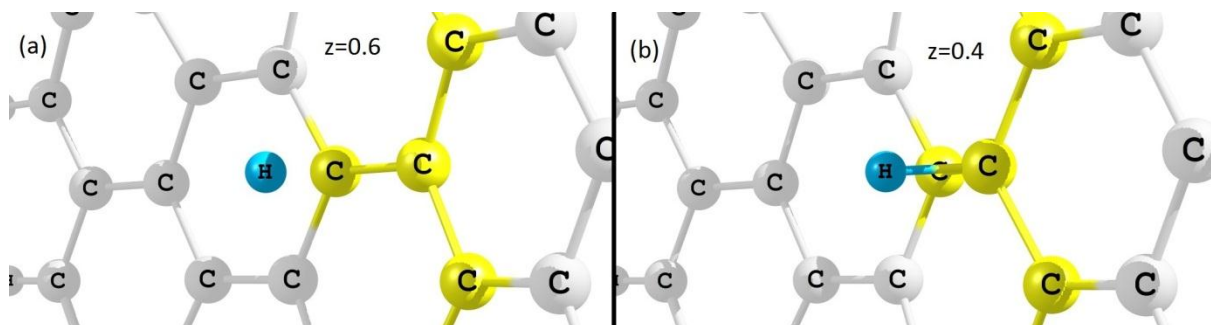


Figure 7: Tetrahedral configuration in vicinity of the permeation site in the middle of the two carbon atoms when the H atom approaches $z=0.4$ Å.

In Fig. 6 the situation is depicted for He permeating different PAH molecules too. It can be observed easily that the agreement between the two methods/basis sets is very good in this case. Since for He repulsion dominates by far, large values of both the total energy (about 16-18 eV) as well as of bond elongation (up to 100%) can be seen.

We note that the shape of the curves seems to depend somewhat on the choice of PAH molecule. Whereas both curves are very similar to those obtained in case of hollow site for anthracene and coronene, the curves for interaction between He and circumpyrene have a different shape. In the latter case, the PAH molecule does not flip back into its original plane after permeation of He, but the two central carbon atoms remain close to He and are indeed following the leaving He atom a bit until the point, where the PAH molecule flips back after all into its original geometry. A reason for this difference may be the greater deformability of circumpyrene where boundary effects are smaller. There the central carbon atoms are pulled back more efficiently from the restricted boundary formed by hydrogen atoms than in case of the smaller PAHs. The circumpyrene curves are likely to be the better models for extended graphene sheets.

The potential energy curves for the interaction of Lithium with the three hydrocarbons (Fig. 6) are very similar to those obtained for the case of helium. Due to convergence problems we are not able to decide if this is also the case for circumpyrene. The maximum values of the total energy are about 12 eV for two functionals and a satisfying convergence with increasing size of the PAH can be observed. The relative change in C-C bond length of the central C-C bond is again rather large, up to 120%.

The most interesting features concerning Be permeating through PAH molecules at the bridge site are the differences between the results obtained with the B3LYP and PBE0 functionals. The total energy barriers as well as the change in C-C bond length of the central C-C bond where the permeation takes place are depicted in Fig. 6. It can be observed that in case of the coronene molecule both the total energy curve as well as the curve concerning change in C-C bond length differ completely. The calculations with different methods also result in a different behavior of coronene when beryllium permeates it. In case of PBE0 the Be atom just moves between the two carbon atoms forming the central C-C bond, whereas in case of B3LYP the Be atom pushes aside this central bond together with both carbon atoms as a whole, see Fig. 8. In the former case, this results in an energy maximum at about 8.5 eV and large separation of the two considered carbon atoms, reflected by the relative change of bond length of about 100%. In the latter case, an even larger energy maximum at about 11 eV is found at $z=2.4$ Å, together with a very small extension or even shortening of the central C-C bond. In both cases, coronene reestablishes its original geometry at the end. Convergence problems prevented us to compare with circumpyrene and anthracene for distances larger than 0.8 Å after permeation. The rise of C-C bond length change for that case, at least, indicates that here the behavior is comparable to the results of PBE0, however, accompanied by a larger energy maximum greater than or equal to about 12 eV. In both cases as well as for circumpyrene, it is again found that for B3LYP the repulsion starts earlier than for PBE0.

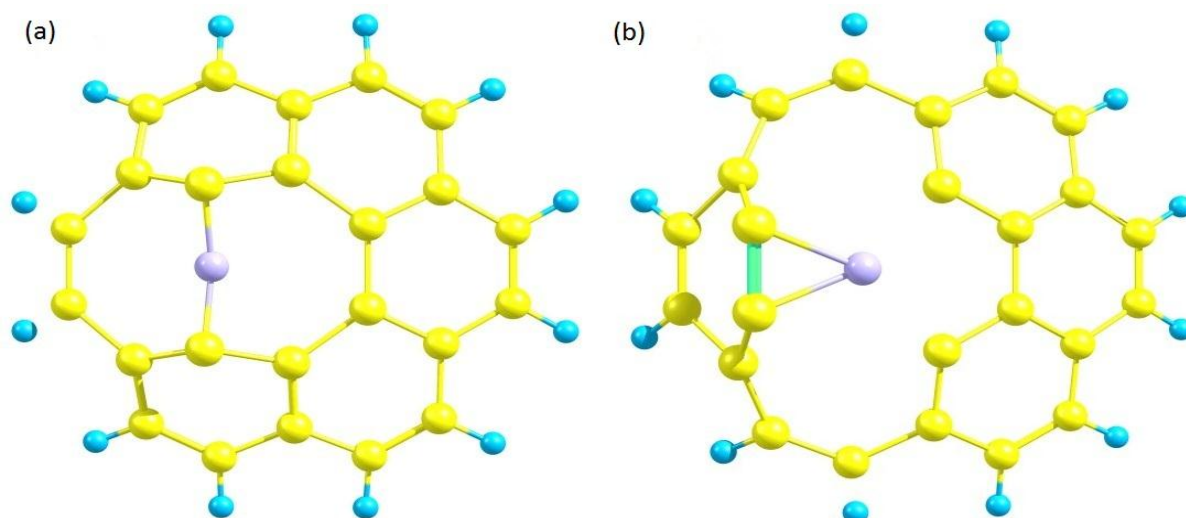


Figure 8: Deformation of coronene due to permeation of Be at bridge site, once obtained with (a) PBE0 and once with (b) B3LYP.

3.4 Adiabatic permeation at top site

In the third geometry investigated the contaminant atom is located on top of a carbon atom. The change of the length of one C-C bond between the carbon at the interaction site and one of its neighbors with the largest deviation from undisturbed bond length has been chosen as a measure of the PAH distortion. In general, permeation at top site leads to more repulsive energy curves as the other geometries and can be imagined to proceed as follows: The contaminant atom first pushes the carbon atom at the permeation site simply out of the undisturbed molecular plane. Due to physical or purely numerical asymmetries the carbon atom starts to be pushed aside as the z-coordinate of the contaminant atom is increased. As the contaminant atom leaves the deformed PAH molecule, the carbon atom flips back into the original position.

We start with the results for the H-PAH system (Fig. 9). As for the permeation at bridge site there exist additional minima in energy as well as non-monotonous bond length changes. They are less pronounced than in the bridge sites but like there they are caused by C-H bond formation. The results from the functionals do not agree as well as for the other geometries. The respective maxima are 8 eV for PBE0 and 9 eV for B3LYP, both at about 0.6 Å. The relative change in C-C bond length is 60-80%. Due to convergence problems we could not obtain results for circumpyrene with the PBE0 functional. The small minima in front of the barrier (at about $z = -1.4$ to -1.2 Å) correspond within 0.2 eV to activation barriers and adsorption minima discovered by earlier DFT studies [24-26, 33] and experiments [46] which focused on chemisorption. The carbon atom extrudes of the PAH plane and a tetrahedral configuration is formed with its neighbors and the approaching hydrogen atom.

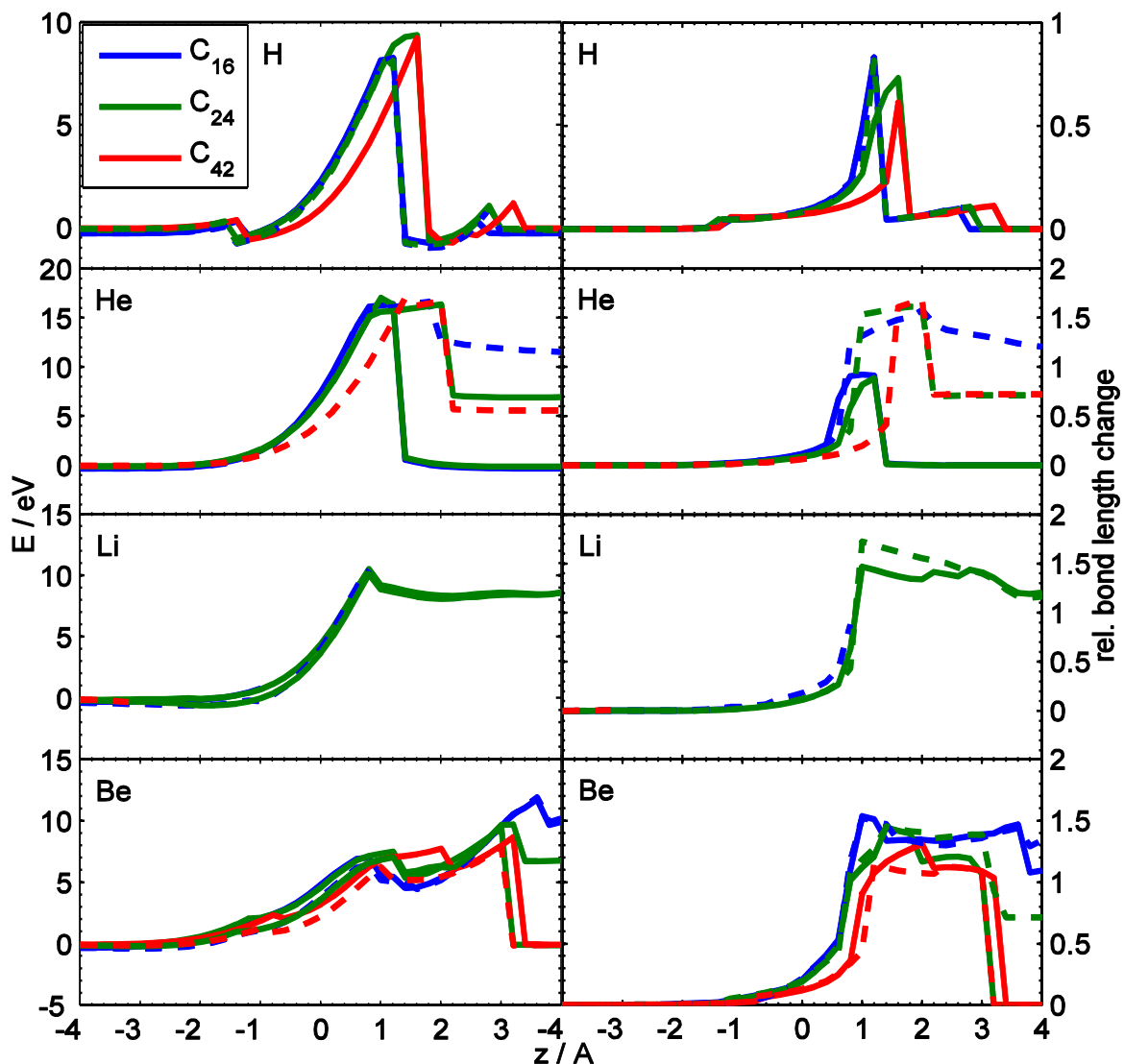


Figure 9: Energy barriers and relative change in C-C bond length in the vicinity of the permeation site for adiabatic permeation through anthracene (blue), coronene (green) and circumpyrene (red) at the top site for H, He, Li and Be. Solid lines are for B3LYP and dashed lines for PBE0.

For permeation of helium through PAH molecules at top site, B3LYP gives results similar to He. For PBE0 the PAH molecules do not relax back into their original geometrical structure. In terms of the energy barrier this leads to a larger total energy at the end of the scan (Fig. 9). The reason for is that the central carbon atom in anthracene remains away from the original plane while coronene and circumpyrene change their structure (Fig. 10). Three coronene hexagons convert into two pentagons and one heptagon while in circumpyrene the four central hexagons are replaced by two pentagons and two heptagons. This isomerization gives also rise to a change in the electronic structure and material properties [47] and is prototypical for a beginning degradation of the surface material.

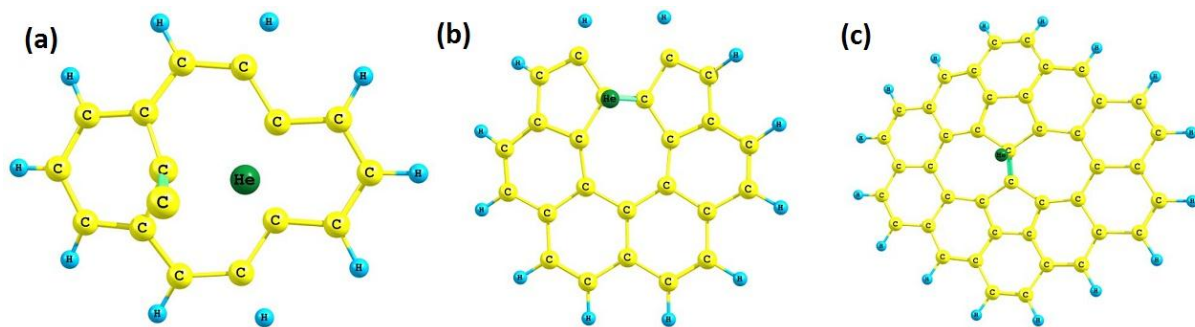


Figure 10: Remaining geometrical structures of anthracene (a), coronene (b) and circumpyrene (c) after permeation of He (dark green) through the molecule at top site.

We discuss only the Li-coronene system. Li pushes the C atom out of molecular plane. Slight asymmetries in geometries and forces cause it to be pushed aside. It also does not flip back after permeation of Li but instead follows it, which further increases the deformation. Consequently, the C-C bond length changes by up to 170% (Fig. 9).

For Be, the situation is even more complicated (Fig. 9). The reason for the two pronounced maxima in energy and rectangular shapes can be rationalized as follows: The central carbon atom is pushed out and to the side. When this carbon atom flips partially back, the energy of the system is reduced, but this carbon forms a C-C bond perpendicular to the original PAH plane. As the contaminant atom leaves the PAH, this out-of-plane bond can return into the original molecular plane. This process is representative for the energy profiles shown in Fig. 9 even though they differ in details from each other.

We conclude this section by summarizing the values for energy maxima and the maxima in relative change in C-C bond length in Table 2. We note that permeation of atoms through coronene requires least energy at hollow site, except for hydrogen, which permeates most easily at bridge site. The energy maxima differ substantial for the case of helium. There the bridge and top site maxima are about 6-7 eV larger in value than at hollow site. For Li and Be the values are rather similar and the differences between the different sites are about 2-3 eV. The value for hydrogen at top site is comparable to those of Li and Be, and substantially (4-5 eV) larger than the values at bridge and hollow site. The maxima in relative change in C-C bond length are very small at hollow site (5-20%) compared to those at bridge and top site, where they are around 100%. Isomerizations of the PAH are found, for example, in case of He at top site for PBE0 and in case of Be at bridge site for B3LYP.

Table 2: Values for energy maxima, E_{\max} [eV] and maxima for relative change of C-C bond length, D_{\max} [%] for permeation through coronene of the atoms H to Be at the three high symmetry sites hollow, bridge and top. Values are given for both methods in use in the following order: B3LYP/PBE0.

	H	He	Li	Be
E_{\max} at H site	5.7/-	10.6/10.7	7.9/7.8	8.1/7.6
E_{\max} at B site	4.5/4.5	16.6/16.8	-/12.3	11.2/8.6
E_{\max} at T site	9.4/8.1	17.1/16.4	10.6/10.2	9.4/9.8
D_{\max} at H site	5.2/-	11.5/12.2	12.1/13.5	16/16.8
D_{\max} at B site	73/82	94/97	-/122	15/97
D_{\max} at T site	73/82	89/161	147/172	144/145

3.5 Comparison of different regimes

As outlined in section III B, in addition to the adiabatic interaction regime, two other regimes were investigated. In the ‘in-plane regime’ the PAH is restricted to stay planar. This relates to a model of graphene that is restricted to planarity by external forces. In the ‘ultra-fast regime’ no relaxation of the PAH is allowed at all, modeling thereby their behavior upon impact of atoms with very high velocities. Since both restrictions lead to much closer approaches between the contaminant atom and carbons of the PAH molecules, only permeations at the hollow site make sense and have been investigated. We also restricted our calculations to coronene. By definition, the energy barriers and deformation curves for these two regimes are symmetric with respect to $z=0$, except for small numerical artifacts and no ‘hysteresis’ occurs. Energies and C-C bond length changes in all three regimes are shown in Fig. 11.

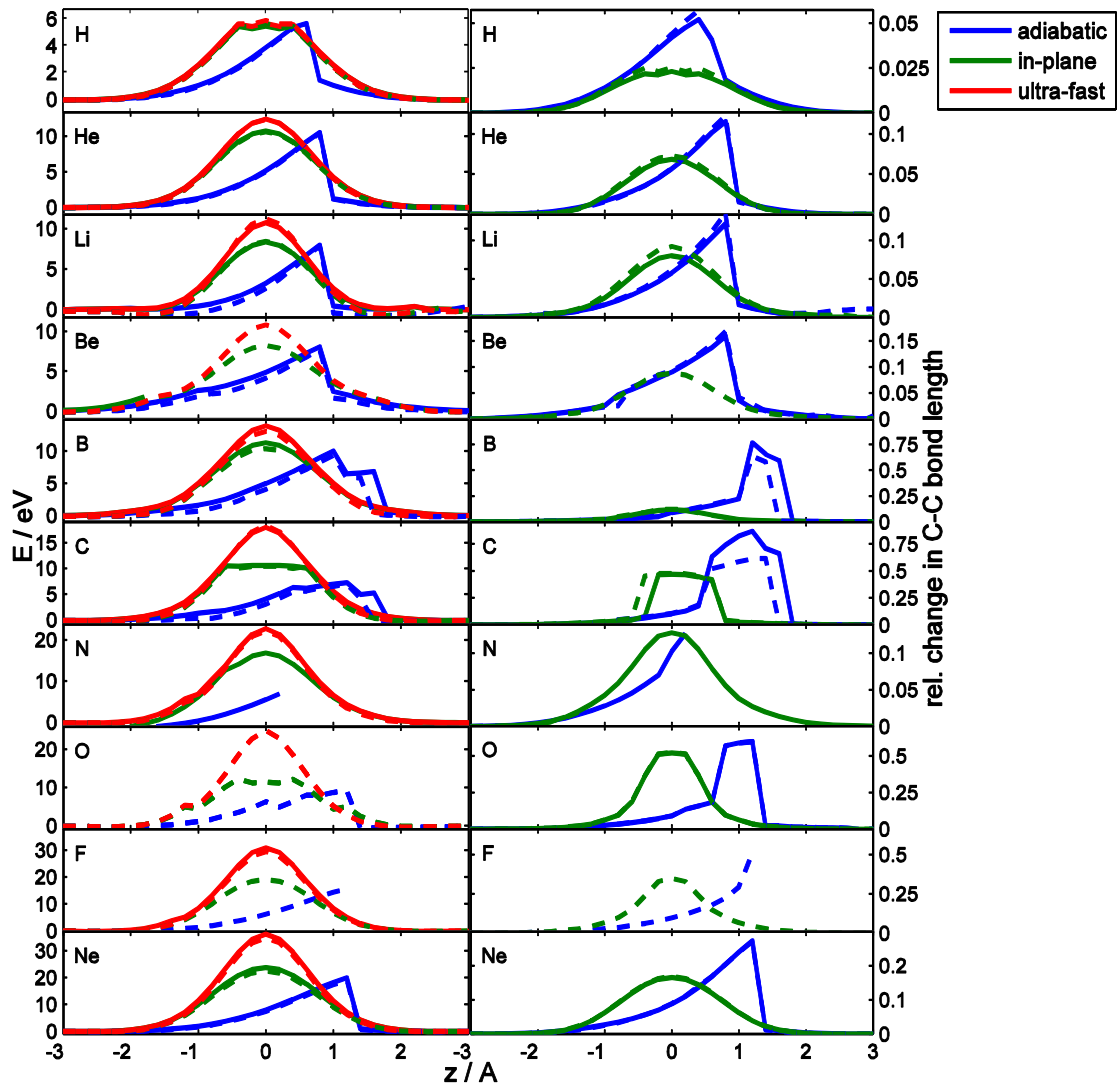


Figure 11: Energy barriers (left) and deformation curves (right) for the adiabatic (blue), in-plane (green) and ultra-fast (red) interaction regimes. Results are shown for B3LYP (solid lines) and PBE0 (dashed lines).

Interestingly, the heights of the planar and adiabatic energy profiles are quite similar, except for carbon and oxygen. This indicates that the out-of-plane stabilization energy is small. Obviously, the contrary is true for the relative change in C-C bond length in the vicinity of hollow site. There, the planar part is lower, about 1/2-2/3, of the adiabatic change in bond length. Both functionals yield very similar results. The energy and deformation

curves for the in-plane and ultra-fast regimes are characterized by their maxima (Table 3). The dependence of the barrier height on the atomic number for the three regimes discussed in this paper is depicted in Fig. 12.

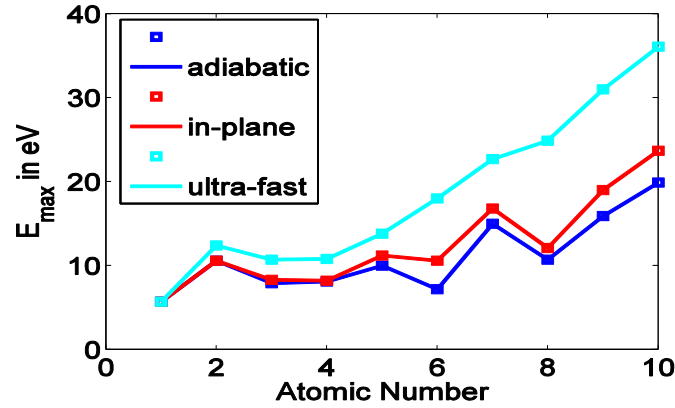


Figure 12: Dependence of the energy barrier height on the atomic number of the atom permeating through coronene at hollow site for the adiabatic (blue), in-plane (red) and ultra-fast (cyan) regime.

Table 3: Values of the energy maxima, E_{\max} [eV] and maxima for relative change of C-C bond length, D_{\max} [%] for permeation of H to Be through coronene at hollow site for in-plane (top) and ultra-fast (bottom) interaction regime. Values are given for the B3LYP/PBE0 functionals.

	H	He	Li	Be	B	C	N	O	F	Ne
E_{\max}	5.7/5.6	10.6/10.7	8.3/8.4	-/8.2	11.2/10.4	10.6/10.4	16.8/-	-/11.3	-/19	23.7/22.4
D_{\max}	2.3/2.5	6.8/7.2	8.0/9.1	-/8.8	11.9/12.3	47/48	12.7/-	-/52	-/35	17/17
E_{\max}	5.7/5.9	12.4/12.4	10.7/11.2	-/10.8	13.8/13	18/18.4	22.7/22	-/25	30.8/29.5	36.1/34.5

3.6 Hydrogenated surfaces

We also explore the adiabatic interaction of these atoms with the 100% hydrogenated version of coronene as a model for graphane (CHC) [38]. The hollow interaction site is still well defined as the midpoint of one of the carbon hexagons which are now puckered. This system is important for fusion research since strongly hydrogenated graphitic surfaces occur in fusion experiments using graphitic plasma facing component (PFC) materials [5]. Indeed, it can be expected that H-covered surfaces are often more abundant than bare ones.

For C, N, O, and F no suitable results could be obtained due to convergence problems. The atoms most relevant concerning nuclear fusion H, He and Be as well as B, Li and Ne have been investigated, however.

As in the case of adiabatic permeation through PAH molecules we can decompose the results for energy barriers and deformation curves in simple ones for H, He, Li, and Ne and more complex ones for Be and B. In the former case the total energy barriers and deformation curves are very much like those for permeation through PAH molecules concerning their shape, with slightly different values of energy barriers and deformation maxima. It turns out that the barriers are slightly reduced, compared to the pure PAHs while the C-C bond length changes are about the same. The results are shown in Fig. 13.

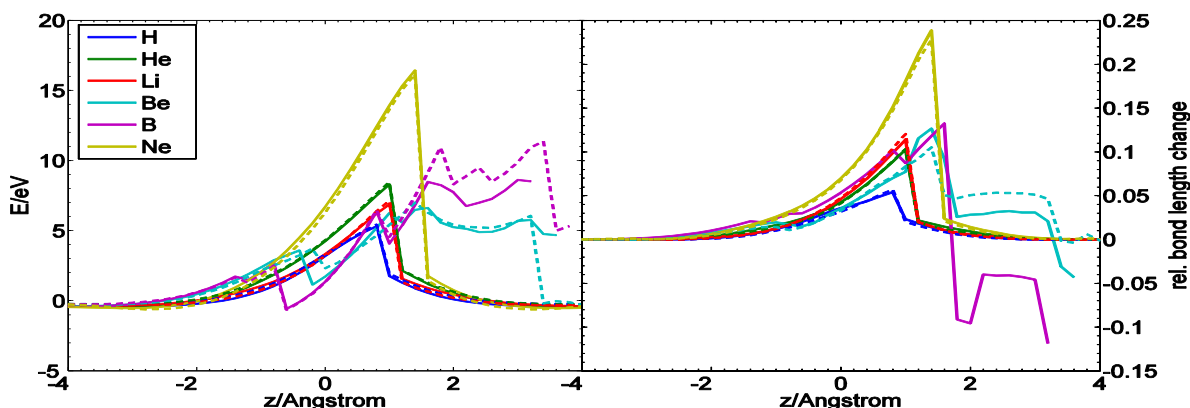


Figure 13: Energy barriers (left) and deformation curves (right) for adiabatic permeation of H (blue), He (green), Li (red), Be (turquoise), B (violet) and Ne (gold) through 100% hydrogenated coronene. Results are shown for B3LYP (solid lines) and PBE0 (dashed lines).

The situation is different when Be and B are contaminant atoms since they form bonds to the CHCs. Their energy barriers and deformation curves are complex and zagged (see Fig. 13) but are similar to each other. In both cases, we observe three maxima in the energy barriers correspond to the three layers (H, then C, then H again) the atoms are permeating through. The additional small maxima visible in some of these curves are thought to be numerical artifacts. A hydrogen molecule is released from the C-H-cluster when the contaminant atom permeates hydrogenated coronene.

4. Conclusions

We investigated the interaction of low-Z atoms H up to Ne with PAH molecules as models for graphitic (0001) surfaces by means of DFT methods using the B3LYP and PBE0 functionals. From these calculations we derived energy barriers and curves characterizing the deformation of the PAH molecules for permeation of the atoms under consideration through the hydrocarbon molecules at different high-symmetry sites. Overall, both functionals gave similar results. An accuracy of about 10-15% concerning the barrier height can be achieved with these functionals in conjunction with the small split-valence basis sets 3-21G and 6-31G. The convergence of the energy barriers with the molecular size of the PAHs shows that they can be used for the present purposes. Thus, the geometric and energetic characterization of atomic interaction with graphitic surfaces can be done on a quantum chemical level by investigating the atomic interaction with PAH molecules of at least the size of coronene.

Based on these findings we derived barrier heights for atomic interaction at the three different high symmetry sites hollow, bridge and top concerning H, He, Li and Be and at hollow site concerning also B, C, N, O, F and Ne. These barrier heights reflect the energy needed to permeate through the surface layer and diffuse into the bulk. Furthermore, we calculated these barriers for three interaction regimes, the adiabatic, in-plane and the ultra-fast one.

The barrier height of about 5 eV for permeation of hydrogen through graphite (0001) surfaces fits well to a peak in adsorption at this energy reported in earlier MD simulations [18] as well as to earlier DFT studies [25]. The large barriers encountered by helium and neon may be a reason of their minor role in sputtering of graphite or derivatives [27]. Together with the shape of the energy barriers, future investigations can lead to improved analytical potential energy functions for molecular dynamics simulations. This might be useful for plasma wall interaction topics such as tritium retention or simply to model the composition of originally pure graphite exposed to an ITER-like mixed material scenario.

Especially for the close relation to nuclear fusion concerns, we also investigated atomic interaction with 100% hydrogenated coronene. We found that in this case the energy barriers heights are slightly lower than for pure coronene.

Similar investigations concerning noble gases, tungsten and small molecules as CH_x , $x=1-4$, and/or BeH_x , $x=1,2$, are in progress [48].

Acknowledgements

This work, supported by the European Commission under the Contract of Association between EURATOM and the Austrian Academy of Sciences, was carried out within the framework of the European Fusion Development Agreement. The views and opinions expressed herein do not necessarily reflect those of the European Commission. This work was supported by the Austrian Ministry of Science BMWF as part of the Uni-Infrastrukturprogramm of the Forschungsplattform Scientific Computing at LFU Innsbruck. Support from the DK+ on computational interdisciplinary modeling and from the RFBR-FWF project 09-03-91001-a is also gratefully acknowledged.

References

- [1] J. Roth, E. Tsitrone, A. Loarte, Plasma-wall interaction: a complex combination of surface processes critical for thermo-nuclear fusion, *Journal of Physics: Conference Series*, 100 (2008).
- [2] V. Philipps, Plasma-wall interaction, a key issue on the way to a steady state burning fusion device, *Physica Scripta*, T123 (2006) 24-32.
- [3] B. Lipschultz, X. Bonnin, G. Counsell, A. Kallenbach, A. Kukushkin, K. Krieger, A. Leonard, A. Loarte, R. Neu, R.A. Pitts, T. Rognlien, J. Roth, C.H. Skinner, J.L. Terry, E. Tsitrone, D. Whyte, S. Zweben, N. Asakura, D. Coster, R. Doerner, R. Dux, G. Federici, M. Fenstermacher, W. Fundamenski, P. Ghendrih, A. Herrmann, J. Hu, S. Krashennnikov, G. Kirnev, A. Kreter, V. Kurnaev, B. LaBombard, S. Lisgo, T. Nakano, N. Ohno, H.D. Pacher, J. Paley, Y. Pan, G. Pautasso, V. Philipps, V. Rohde, D. Rudakov, P. Stangeby, S. Takamura, T. Tanabe, Y. Yang, S. Zhu, Plasma-surface interaction, scrape-off layer and divertor physics: implications for ITER, *Nuclear Fusion*, 47 (2007) 1189-1205.
- [4] U. Samm, Plasma-Wall Interaction in Magnetically Confined Fusion Plasmas, *Transactions of Fusion Science and Technology*, 53 (2008) 223-228.
- [5] G. Federici, C.H. Skinner, J.N. Brooks, J.P. Coad, C. Grisolia, A.A. Haasz, A. Hassanein, V. Philipps, C.S. Pitcher, J. Roth, W.R. Wampler, D.G. Whyte, Plasma-material interactions in current tokamaks and their implications for next step fusion reactors, *Nuclear Fusion*, 41 (2001) 1967-2137.
- [6] M.A. Abdou, A. Ying, N. Morley, K. Gulec, S. Smolentsev, M. Kotschenreuther, S. Malang, S. Zinkle, T. Rognlien, P. Fogarty, B. Nelson, R. Nygren, K. McCarthy, M.Z. Youssef, N. Ghoniem, D. Sze, C. Wong, M. Sawan, H. Khater, R. Woolley, R. Mattas, R. Moir, S. Sharafat, J. Brooks, A. Hassanein, D. Petti, M. Tillack, M. Ulrickson, T. Uchimoto, On the exploration of innovative concepts for fusion chamber technology, *Fusion Engineering and Design*, 54 (2001) 181-247.
- [7] R.W. Moir, Liquid first walls for magnetic fusion energy configurations, *Nuclear Fusion*, 37 (1997) 557-566.
- [8] B. Lipschultz, D.A. Pappas, B. LaBombard, J.E. Rice, D. Smith, S.J. Wukitch, A study of molybdenum influxes and transport in Alcator C-Mod., *Nuclear Fusion*, 41 (2001) 585-596.
- [9] G.L. Jackson, J. Winter, T.S. Taylor, K.H. Burrell, J.C. DeBoo, C.M. Greenfield, R.J. Groebner, T. Hodapp, K. Holtrop, e. al., Regime of very high confinement in the boronized DIII-D tokamak., *Physical Review Letters*, 67 (1991) 3098-3101.
- [10] U. Samm, P. Bogen, G. Esser, J.D. Hey, E. Hintz, A. Huber, L. Koenen, Y.T. Lie, P. Mertens, e. al., Plasma edge physics with siliconization in TEXTOR., *Journal of Nuclear Materials*, 220-222 (1995) 25-35.
- [11] H.G. Esser, S.J. Fielding, S.D. Hanks, P.C. Johnson, A. Kislyakov, J. Winter, Boronization of COMPASS [a tokamak]. *Journal of Nuclear Materials*, 186 (1992) 217-226.
- [12] H.G. Esser, J. Winter, V. Philipps, H.B. Reimer, J. Von Seggern, P. Wienhold, e. al., Plasma discharge fueling by reactive gases., *Journal of Nuclear Materials*, 196-198 (1992) 231-235.
- [13] M.R. Wade, J.T. Hogan, S.L. Allen, N.H. Brooks, D.N. Hill, R. Maingi, M.J. Schaffer, J.G. Watkins, D.G. Whyte, R.D. Wood, W.P. West, Impurity enrichment studies with induced scrape-off layer (SOL) flow on DIII-D., *Nuclear Fusion*, 38 (1998) 1839-1859.
- [14] J.A. Goetz, B. LaBombard, B. Lipschultz, C.S. Pitcher, J.L. Terry, C. Boswell, S. Gangadhara, D. Pappas, J. Weaver, B. Welch, R.L. Boivin, P. Bonoli, C. Fiore, R. Granetz, M. Greenwald, A. Hubbard, I. Hutchinson, J. Irby, E. Marmor, D. Mossessian, M. Porkolab, J. Rice, W.L. Rowan, G. Schilling, J. Snipes, Y. Takase, S. Wolfe, S. Wukitch, High confinement dissipative divertor operation on Alcator C-Mod., *Physics of Plasmas*, 6 (1999) 1899-1906.
- [15] J.A. Goetz, B. Lipschultz, C.S. Pitcher, J.L. Terry, P.T. Bonoli, J.E. Rice, S.J. Wukitch, Impurity compression and enrichment studies on Alcator C-Mod., *Journal of Nuclear Materials*, 266-269 (1999) 354-359.

- [16] J. Rapp, P. Monier-Garbet, P. Andrew, P. Dumortier, T. Eich, W. Fundamenski, M. von Hellermann, J. Hogan, L.C. Ingesson, S. Jachmich, H.R. Koslowski, A. Loarte, G. Maddison, G.F. Matthews, D.C. McDonald, A. Messiaen, J. Ongena, V. Parail, V. Philipps, G. Saibene, R. Sartori, B. Unterberg, Reduction of divertor heat load in JET ELMy H-modes using impurity seeding techniques., *Fusion Energy*, (2003) 1021-1025.
- [17] H.D. Pacher, A.S. Kukushkin, G.W. Pacher, V. Kotov, G. Janeschitz, D. Reiter, D.P. Coster, Impurity seeding and scaling of edge parameters in ITER., *Journal of Nuclear Materials*, 390-391 (2009) 259-262.
- [18] A. Ito, H. Nakamura, Molecular dynamics simulation of collisions between hydrogen and graphite, *J. Plasma Phys.*, 72 (2006) 805-808.
- [19] S.J. Stuart, P.S. Krstic, T.A. Embry, C.O. Reinhold, Methane production by deuterium impact at carbon surfaces, *Nuclear Instruments and Methods in Physics Research B*, 255 (2007) 202-207.
- [20] A. Ito, H. Nakamura, Hydrogen isotope sputtering of graphite by molecular dynamics simulation, *Thin Solid Films*, 516 (2008) 6553-6559.
- [21] A. Ito, H. Nakamura, Molecular Dynamics Simulation of Bombardment of Hydrogen Atoms on Graphite Surface, *Communications in Computational Physics*, 4 (2008) 592-610.
- [22] A. Ito, Y. Wang, S. Irle, K. Morokuma, H. Nakamura, Molecular dynamics simulation of hydrogen atom sputtering on the surface of graphite with defect and edge, *J. Nucl. Mat.*, 390-391 (2009) 183-187.
- [23] A. Ito, K. Ohya, K. Inai, H. Nakamura, Dependency of Tritium Retention in Graphite on Temperature Control of Molecular Dynamics, *Contributions to Plasma Physics*, 50 (2010) 464-469.
- [24] X. Sha, B. Jackson, First-principles study of the structural and energetic properties of H atoms on a graphite (0001) surface, *Surface Science*, 496 (2002) 318-330.
- [25] Y. Ferro, C. Brosset, A. Allouche, Quantum Study of Hydrogen Interaction with Plasma-Facing Graphite and Boron Doped Graphite Surfaces, *Physica Scripta*, T108 (2004) 76-79.
- [26] Y. Ferro, A. Jelea, F. Marinelli, C. Brosset, A. Allouche, Density functional theory and molecular dynamics studies of hydrogen interaction with plasma-facing graphite surfaces and the impact of boron doping, *Journal of Nuclear Materials*, 337-339 (2005) 897-901.
- [27] P. Traeskelin, K. Nordlund, J. Keinonen, H. He, Ne, Ar-bombardment of amorphous hydrocarbon structures, *Journal of Nuclear Materials*, 357 (2006) 1-8.
- [28] P.S. Krstic, C.O. Reinhold, S.J. Stuart, Chemical sputtering from amorphous carbon under bombardment by deuterium atoms and molecules, *New Journal of Physics*, 9 (2007).
- [29] P. Traeskelin, O. Saresoja, K. Nordlund, Molecular dynamics simulations of C₂, C₂H, C₂H₂, C₂H₃, C₂H₄, C₂H₅, and C₂H₆ bombardment of diamond (111) surfaces, *Journal of Nuclear Materials*, 375 (2008) 270-274.
- [30] C. Bjoerkas, K. Voertler, K. Nordlund, D. Nishijima, R. Doerner, Chemical sputtering of Be due to D bombardment, *New Journal of Physics*, 11 (2009) 123017.
- [31] J. Marian, L.A. Zepeda-Rutz, G.H. Gilmer, E.M. Bringa, T. Rognlien, Simulations of carbon sputtering in amorphous hydrogenated samples, *Phys. Scr.*, T124 (2006) 65-69.
- [32] D.W. Brenner, O.A. Shenderova, J.A. Harrison, S.J. Stuart, B. Ni, S.B. Sinnott, A second-generation reactive empirical bond order (REBO) potential energy expression for hydrocarbons, *J. Phys.: Condens. Matter*, 14 (2002) 783-802.
- [33] L. Jeloica, V. Sidis, DFT investigation of the adsorption of atomic hydrogen on a cluster-model graphite surface, *Chemical Physics Letters*, 300 (1999) 157-162.
- [34] L. Hornekaer, E. Rauls, W. Xu, Z. Sljivancanin, R. Otero, I. Stensgaard, E. Laegsgaard, B. Hammer, F. Besenbacher, Clustering of Chemisorbed H(D) Atoms on the Graphite (0001) Surface due to Preferential Sticking, *Physical Review Letters*, 97 (2006) 1-4.
- [35] A. Ishi, M. Yamamoto, H. Asano, K. Fujiwara, *J. Phys.: Conference Series*, 100 (2008).
- [36] X. He, Z. Chen, Z. Li, Z. Zou, *Cond. Mat.*, (2010).
- [37] L. Sheng, Y. Ono, T. Taketsugu, *Journal of Physical Chemistry C*, 114 (2010).
- [38] D.C. Elias, R.R. Nair, T.M.G. Mohiuddin, S.V. Morozov, P. Blake, M.P. Halsall, A.C. Ferrari, D.W. Boukhvalov, M.I. Katsnelson, A.K. Geim, K.S. Novoselov, Control of Graphene's Properties by Reversible Hydrogenation: Evidence for Graphane, *Science*, 323 (2009) 610-613.
- [39] K. Jug, T. Bredow, Models for the Treatment of Crystalline Solids and Surfaces, *Journal of Computational Chemistry*, 25 (2004) 1551-1567.
- [40] A. Becke, Density-functional thermochemistry. III. The role of exact exchange, *Journal of Chemical Physics*, 98 (1993) 5648-5652.
- [41] C. Adamo, V. Barone, Toward reliable density functional methods without adjustable parameters: The PBE0 model, *Journal of Chemical Physics*, 110 (1999) 6158-6170.
- [42] J. Chai, M. Head-Gordon, Long-range corrected hybrid density functionals with damped atom-atom dispersion corrections, *Physical Chemistry Chemical Physics*, 10 (2008) 6615-6620.
- [43] J.S. Birkley, J.A. Pople, W.J. Hehre, *Journal of the American Chemical Society*, 102 (1980).

- [44] R. Ditchfield, W.J. Hehre, J.A. Pople, *Journal of Chemical Physics*, 54 (1971).
- [45] M.J. Frisch, G.W. Trucks, H.B. Schlegel, G.E. Scuseria, M.A. Robb, J.R. Cheeseman, G. Scalmani, V. Barone, B. Mennucci, G.A. Petersson, H. Nakatsuji, M. Caricato, X. Li, H.P. Hratchian, A.F. Izmaylov, J. Bloino, G. Zheng, J.L. Sonnenberg, M. Hada, M. Ehara, K. Toyota, R. Fukuda, J. Hasegawa, M. Ishida, T. Nakajima, Y. Honda, O. Kitao, H. Nakai, T. Vreven, J.A. Montgomery, Jr., J.E. Peralta, F. Ogliaro, M. Bearpark, J.J. Heyd, E. Brothers, K.N. Kudin, V.N. Staroverov, R. Kobayashi, J. Normand, K. Raghavachari, A. Rendell, J.C. Burant, S.S. Iyengar, J. Tomasi, M. Cossi, N. Rega, J.M. Millam, M. Klene, J.E. Knox, J.B. Cross, V. Bakken, C. Adamo, J. Jaramillo, R. Gomperts, R.E. Stratmann, O. Yazyev, A.J. Austin, R. Cammi, C. Pomelli, J.W. Ochterski, R.L. Martin, K. Morokuma, V.G. Zakrzewski, G.A. Voth, P. Salvador, J.J. Dannenberg, S. Dapprich, A.D. Daniels, O. Farkas, J.B. Foresman, J.V. Ortiz, J. Cioslowski, D.J. Fox, *Gaussian 09*, Revision A.1, in, Gaussian, Inc., Wallingford CT, 2009.
- [46] T. Zecho, A. Guettler, X. Sha, B. Jackson, J. Kueppers, *Journal of Chemical Physics*, 117 (2002).
- [47] V.H. Crespi, L.X. Benedict, M.L. Cohen, S.G. Louie, Prediction of a pure-carbon planar covalent metal, *Physical Review B*, 53 (1996) 13303-13305.
- [48] S.E. Huber, M. Probst, in preparation.